Title

Corrigendum: Theoretical and applied research on bistable dual-piezoelectric-cantilever vibration energy harvesting toward realistic ambience (2016 Smart Mater. Struct. 25 115032)

Journal

Smart Materials and Structures, 27(1)

ISSN

0964-1726

Authors

Gao, Y
Leng, Y
Javey, A
et al.

Publication Date

2018

DOI

10.1088/1361-665x/aa98bc

Peer reviewed

Theoretical and applied research on bistable dual-piezoelectric-cantilever vibration energy harvesting toward realistic ambience

Yuji Gao[1, 3, 4, 5], Yonggang Leng[1, 2, a)], Ali Javey[3, 4, 5], Dan Tan[1], Jinjun Liu[1], Shengbo Fan[1], and Zhihui Lai[1]

[1]*School of Mechanical Engineering, Tianjin University, Tianjin 200072, China*

[2]*Key Laboratory of Mechanism Theory and Equipment Design of Ministry of Education, Tianjin University, Tianjin 300072, China*

[3]*Department of Electrical Engineering & Computer Sciences, University of California, Berkeley, CA 94720*

[4]*Berkeley Sensor and Actuator Center, University of California, Berkeley, CA*

[5]*Materials Sciences Division, Lawrence Berkeley National Laboratory, Berkeley, CA*

Abstract: Pink noises, known similar to realistic ambient noises, are normally used to simulate the ambience where the piezoelectric energy harvesting system (PEHS) would be set up. However, pink noises with standard spectral representation can only be used for simulation on excitations that are assumed to own constant intensity, while realistic ambient noises normally come along with random spectrum and varying intensity in terms of different locations and time period. The output performance of the conventional bistable magnetic repulsive energy harvesters would be significantly affected by the intensity of ambience. Considering this, a model of bistable dual-piezoelectric-cantilever energy harvester (DPEH) is established in this paper to achieve optimal broadband energy harvesting toward varying-intensity realistic circumstance. We utilized a variety of realistic ambient conditions as excitations to obtain the energy harvesting performance of DPEH for theoretical and applied study. It has been proven that the elastic-supported piezoelectric energy harvesting system (EPEHS) is more adaptive to realistic ambience with significant or medium intensity variation, while less qualified toward the realistic ambience with constant intensity than the rigid-supported piezoelectric energy harvesting system (RPEHS). Fortunately, the dual-piezoelectric-cantilever energy harvesting system (DPEHS) is superior to RPEHS under all circumstance due to the dual piezoelectric cantilevers of being efficiently utilized for electromechanical energy conversion so as to accomplish optimal energy harvesting.

Keywords: Energy harvesting; Bistable oscillation; Dual-piezoelectric-cantilever; Varying-intensity; Realistic ambience

---

[a)] Correspondence should be addressed to Yonggang Leng (leng_yg@tju.edu.cn).

1. Introduction

Piezoelectric energy harvesting systems (PEHS) has been extensively investigated in the past decades as a renewable alternative to batteries for the use of power supply for low-power electronics such as wireless sensor networks and self-sustained electronic components. The mechanism to realize this relies on a conversion from ambient vibrational energy to electrical energy due to the piezoelectric effect by piezoelectric crystals. PEHS has the advantages of high energy density, simple structures, and ease of being embedded in micro-electromechanical systems (MEMS). [1, 2] A conventional linear piezoelectric energy harvester (PEH) prototype is typically based on a cantilever attached with piezoelectric patches and a tip proof mass. The cantilever structure is utilized to incur deformation of piezoelectric ceramics for electric charge generation while the proof mass aims to decrease the inherent frequency for environmental catering, since it requires the linear PEH to be under resonance for optimal oscillations to occur. However, the frequency spectrum of ambience is with low frequency broadband, which disqualifies the linear PEH in extensive applications.[3]

To broaden the bandwidth, many approaches like discrete arrays and frequency tuning technologies have been contributed by researchers.[4, 5] Other than these methods, nonlinear PEHS appeared to realize effective broadband response. To date, researchers have exploited various approaches to introduce nonlinearity into energy harvesting for theoretical analysis and application exploration, including monostable Duffing, bistable oscillators, etc. Ramlan *et al*.[6] investigated the potential benefits of nonlinear stiffness in a monostable Duffing energy harvester. Mann and Sims[7] established a Duffing electromagnetic oscillator that uses magnetic levitation to realize resonance tuning. A piezoelectric electromechanical coupled Duffing oscillator was investigated by Sebald *et al*.[8] Typical approaches to generate bistability are mainly based on magnetic attraction, magnetic repulsion, buckled beams and bistable plates. Bistable dynamics caused by magnetic attraction is revealed by Erturk *et al*.[9] and Zhao *et al*.[10] using a piezomagnetoelastic structure for harmonic excitation. In terms of bistable behaviors caused by magnetic repulsion, Cottone *et al*.[11] and Ferrari *et al*.[12] explored the performance under noise excitations which was proven to receive 400%-600% enhancement compared to linear counterparts. Another bistable inertial oscillator under sweep excitations was studied by Stanton *et al*.[13] The investigation of a bistable electromagnetic harvester that uses magnetic interactions was explored by Mann and Owens[14] toward chirp excitations. As for buckled beam bistable oscillators, Cottone *et al*.[15] investigated the buckling bistability of a preloaded piezoelectric beam. Liu *et al*.[16] exhibited a buckled spring-mass architecture to observe performance under chirp and band-limited noise excitations. An M-shaped structure proposed by Leadenham *et al.*[17] paid attention to energy harvesting enhancement under low vibration levels. Other than aforementioned bistable studies, a bistable plate was introduced by Arrieta *et al.*[18] for broadband nonlinear energy harvesting.

Among current nonlinear oscillator investigations[6-22], bistable dynamics caused by magnetic repulsion has been attracting lots of interests. A conventional bistable magnetic repulsive PEH is composed of a piezoelectric cantilever with an internal magnet fixed to its free end and an external rigid-supported repulsive magnet, which contributes in forming two wells for bistable oscillations.[23] With respect to vibration source, filtered Gaussian noises or pink noises are normally used to simulate the ambience where the PEH would be set up.[24, 25] Those types of noises have common low-frequency features which makes them proper candidates to simulate the ambient noises. Rather than filtered Gaussian noises, pink noises, whose power spectral density (PSD) is inversely proportional to frequency, are known more similar to realistic ambient noises, since this feature can also be generally found in ambient signals.[26-28] However, pink noises with standard spectral representation can only be used for simulation on excitations that are assumed to own constant intensity, while realistic ambient noises normally come along with random spectrum and varying intensity in terms of different locations and time period.

Unfortunately, the output performance of the conventional bistable magnetic repulsive energy harvesters would be significantly affected by the intensity of ambience. Insufficient intensity may lead to weak oscillations limited in either well instead of bistable transition oscillations between two wells, which would eventually result in lack of adequate energy harvesting. To overcome this defect of the conventional rigid-supported piezoelectric energy harvester (RPEH), an elastic-supported model has been established in our previous work to guarantee persistent bistable oscillations toward varying-intensity excitation conditions.[25, 29] One typical approach to realize this elastic-supported model is to have the external magnet supported by a cantilever. Under such circumstances, it would not be difficult to come up with a proposal that is to deposit piezoelectric ceramic films (PZT) onto the external cantilever for valid electromechanical energy conversion as well. Therefore, a model of dual-piezoelectric-cantilever energy harvester (DPEH) is established in this paper to achieve optimal broadband energy harvesting toward varying-intensity realistic circumstance. It has already been proven in our previous work that the elastic-supported piezoelectric energy harvester (EPEH) is adaptive to filtered Gaussian noises or pink noises with variable intensity.[25] Based on this, in this paper we are inclined to go through a variety of realistic ambient conditions to be used as excitations to observe the energy harvesting performance of DPEHS for theoretical and applied study.

2. Mechanisms

The schematic of DPEH is exhibited in Fig. 1. The model is composed of two piezoelectric cantilevers aligned along Y and Z axis with two permanent magnets (A and B) attached to their free ends facing each other in a repulsive position, which contributes in forming two wells for each piezoelectric cantilever so as to perform dual-bistable function. Each piezoelectric cantilever specifically demands a metal substrate partially sandwiched between a pair of serial piezoelectric patches which would play roles of electric charge generation during oscillation process. The established model presents functionality by transferring ambient mechanical excitations applied on a base where the two piezoelectric cantilevers are rooted in along Z axis into electrical output due to deformation of piezoelectric ceramics via piezoelectric effect. Compared to a conventional rigid-supported model, the benefit of having the external magnet elastically supported by a piezoelectric cantilever is to get higher transition probability, which is due to the dual-bistability with varying potential functions.[25] It should be noted that the gravity direction is along X axis thus the gravity effect can be ignored.

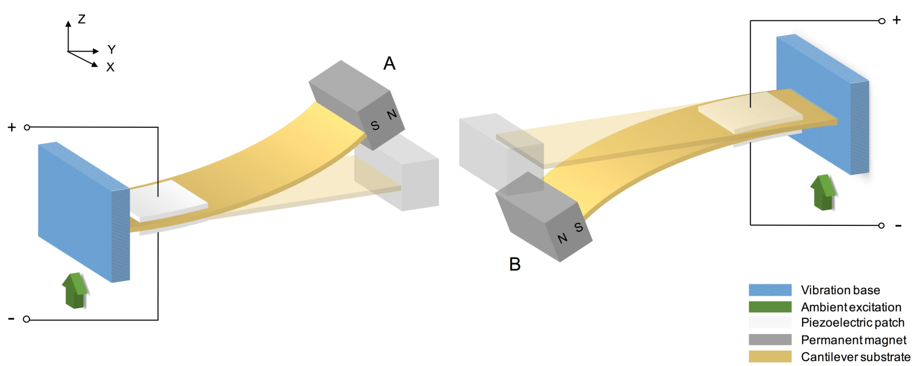

FIG. 1. Schematic of DPEH.

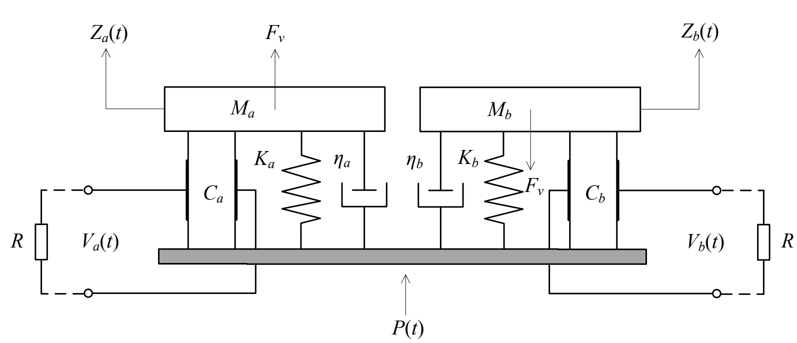

FIG. 2. Equivalent model of DPEH.

As for lumped system analysis, an equivalent mass-spring-damper model could be derived, as shown in Fig. 2, with corresponding dynamic equations:

$$k_a P(t) + \theta V_a(t) + F_v = M_a \ddot{Z}_a(t) + \eta_a \dot{Z}_a(t) + K_a Z_a(t) \tag{1a}$$

$$k_b P(t) + \theta V_b(t) - F_v = M_b \ddot{Z}_b(t) + \eta_b \dot{Z}_b(t) + K_b Z_b(t) \tag{1b}$$

where M, K, and η, respectively, represent the equivalent mass, equivalent stiffness, and equivalent damping; θ is the electromechanical coupling coefficient of PZT; k is the amplitude correction factor in lumped parameter models; $P(t)$ represents the ambient vibrations during a period of time t ; F_v is the vertical component of magnetic repulsive force F; $Z(t)$ represents the vertical displacement of the corresponding magnet; and $V(t)$ is the output voltage of PZT. a and b, respectively, represent the internal (left) and external (right) part of the system while applying for all relevant symbol subscripts in the text.[30-33]

On the basis of *Kirchhoff's first law*, the equations of acquisition circuit are described by [33]

$$\theta \dot{Z}_a(t) + \frac{1}{2} C_a V_a(t) + \frac{V_a(t)}{R} = 0 \tag{2a}$$

$$\theta \dot{Z}_b(t) + \frac{1}{2} C_b V_b(t) + \frac{V_b(t)}{R} = 0 \tag{2b}$$

where R is the resistive load and C is the coupling capacitance. $Z(t)$ and $V(t)$ can be derived from Eqs. (1) and (2) using the *Runge-Kutta method*.[34-36]

The magnetic force is demonstrated using the vector differentiation approach.[11, 37] Under assumed boundary conditions, magnets A and B can be simplified, respectively, as dipoles A and B. The magnetic induction generated by dipole B at the location of dipole A is given by

$$\boldsymbol{B}_{BA} = -\frac{\mu_0}{4\pi} \boldsymbol{\nabla} \frac{\boldsymbol{m}_B \cdot \boldsymbol{r}}{r^3} \tag{3}$$

where $\boldsymbol{m}_B$ is the magnetic moment of dipole B, and $\boldsymbol{r}$ is the vector from the center of magnetic dipole B to the center of dipole A.

The magnetic potential energy and force exerted by dipole B on dipole A can be defined as follows:

$$U_A = -\boldsymbol{B}_{BA} \cdot \boldsymbol{m}_A \tag{4}$$

$$\boldsymbol{F} = -\boldsymbol{\nabla} U_A = -\frac{\mu_0}{4\pi} \boldsymbol{\nabla} \left[\left(\boldsymbol{\nabla} \frac{\boldsymbol{m}_B \cdot \boldsymbol{r}}{r^3} \right) \cdot \boldsymbol{m}_A \right] \tag{5}$$

where $\boldsymbol{m}_A$ is the magnetic moment of dipole A.

Using the following gradient functions:

$$\nabla \frac{1}{r^n} = \begin{pmatrix} \partial/\partial x \\ \partial/\partial y \\ \partial/\partial z \end{pmatrix} \frac{1}{r^n} = -\frac{n}{r^{n+1}} \begin{pmatrix} x/r \\ y/r \\ z/r \end{pmatrix} = -\frac{n\boldsymbol{r}}{r^{n+2}} \tag{6}$$

$$\nabla(\boldsymbol{v}_1 \cdot \boldsymbol{r}) = \begin{pmatrix} \partial/\partial x \\ \partial/\partial y \\ \partial/\partial z \end{pmatrix} (\boldsymbol{v}_1 \cdot \boldsymbol{r}) = \begin{pmatrix} \partial/\partial x(x_1 x + y_1 y + z_1 z) \\ \partial/\partial y(x_1 x + y_1 y + z_1 z) \\ \partial/\partial z(x_1 x + y_1 y + z_1 z) \end{pmatrix} = \begin{pmatrix} x_1 \\ y_1 \\ z_1 \end{pmatrix} = \boldsymbol{v}_1 \tag{7}$$

where $\boldsymbol{v}_1$ is a certain vector, Eq. (5) can be simplified as follows:

$$\boldsymbol{F} = \frac{3\mu_0 m_A m_B}{4\pi r^4}[\hat{\boldsymbol{r}}(\hat{\boldsymbol{m}}_A \cdot \hat{\boldsymbol{m}}_B) + \hat{\boldsymbol{m}}_B(\hat{\boldsymbol{m}}_A \cdot \hat{\boldsymbol{r}}) + \hat{\boldsymbol{m}}_A(\hat{\boldsymbol{m}}_B \cdot \hat{\boldsymbol{r}}) - 5\hat{\boldsymbol{r}}(\hat{\boldsymbol{m}}_A \cdot \hat{\boldsymbol{r}})(\hat{\boldsymbol{m}}_B \cdot \hat{\boldsymbol{r}})] \tag{8}$$

where $\hat{\boldsymbol{r}}$, $\hat{\boldsymbol{m}}_A$, and $\hat{\boldsymbol{m}}_B$, respectively, represent the unit vectors along the direction of $\boldsymbol{r}$, $\boldsymbol{m}_A$, and $\boldsymbol{m}_B$, while r, m_A, and m_B, respectively, represent the corresponding length.

In terms of our dual-piezoelectric-cantilever model, the vertical component of the magnetic force varies with the vertical displacements and the relative position of the two magnets, as shown in Figs 1 and 3, which is given by

$$F_v = \frac{3\mu_0 m_A m_B}{4\pi r^4}[(\cos\theta - 5\cos\alpha\cos\beta)\cos\delta + \cos\alpha\sin\gamma + \cos\beta\sin\varphi] \tag{9}$$

where α is the angle between $\boldsymbol{m}_A$ and $\boldsymbol{r}$, β is the angle between $\boldsymbol{m}_B$ and $\boldsymbol{r}$, θ is the angle between $\boldsymbol{m}_A$ and $\boldsymbol{m}_B$, φ is the angle between $\boldsymbol{m}_A$ and the horizontal direction, γ is the angle between $\boldsymbol{m}_B$ and the horizontal direction, δ is the angle between $\boldsymbol{r}$ and the vertical direction, as shown in Fig. 3. $\boldsymbol{m}_A$ and $\boldsymbol{m}_B$ are respectively given by $m_A = M_A V_A$ and $m_B = M_B V_B$, where M_A and M_B, respectively, represent the magnetization of the two magnets; V_A and V_B, respectively, represent the volume of the two magnets; M_A can be estimated as $M_A = B_r/\mu_0$; $M_A = M_B$, and $V_A = V_B$; B_r is the residual flux density of the permanent magnets, and μ_0 is the permeability of vacuum.

Meanwhile, we can derive the magnetic potential energy expression of U_A:

$$\begin{aligned} U_A &= \frac{\mu_0 m_A m_B}{4\pi r^3}[\hat{\boldsymbol{m}}_A \cdot \hat{\boldsymbol{m}}_B - 3(\hat{\boldsymbol{m}}_A \cdot \hat{\boldsymbol{r}})(\hat{\boldsymbol{m}}_B \cdot \hat{\boldsymbol{r}})] \\ &= \frac{\mu_0 m_A m_B}{4\pi r^3}(\cos\theta - 3\cos\alpha\cos\beta) \end{aligned} \tag{10}$$

Without consideration of gravity, the potential energy of the internal (left) part of the system, including the elastic potential energy and the magnetic potential energy, is given by

$$\begin{aligned} U_a(Z_a, Z_b) &= U_{K_a}(Z_a) + U_A(Z_a, Z_b) \\ &= \frac{1}{2}K_a {Z_a}^2 + \frac{\mu_0 m_A m_B}{4\pi r^3}(\cos\theta - 3\cos\alpha\cos\beta) \end{aligned} \tag{11}$$

The dependence of the potential energy in the internal (left) part of DPEHS (U_a) on the vertical displacements of both magnets (Z_a and Z_b) with certain parameters is shown in Fig. 4 for general comprehension. Apparently as shown, different from the situation in RPEHS ($Z_b = 0$), U_a in DPEHS has varying potential wells along with the variation of Z_b, which would change randomly during oscillation process. This property of DPEHS would help provide higher transition probability to guarantee bistable performance.

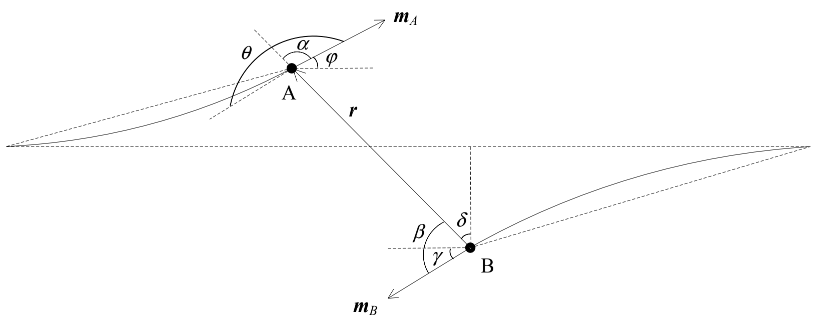

FIG. 3. Geometries of the two magnetic dipoles.

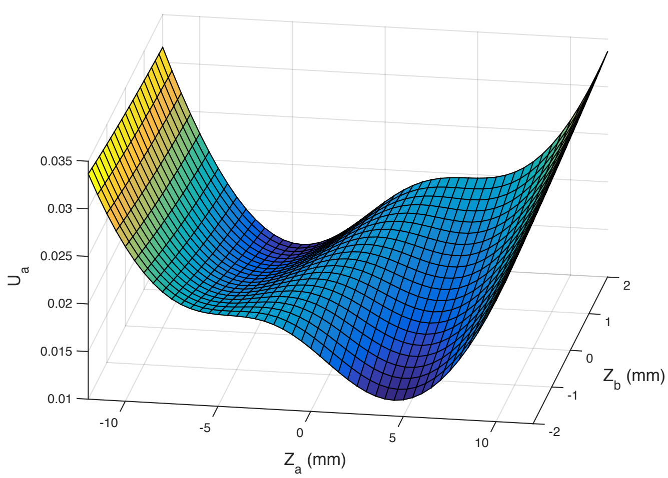

FIG. 4. Variation trend of the potential energy in the internal (left) part of DPEHS.

3. Power output performance

A DPEH device was fabricated using the parameters in Tables 1 and 2 for experimental analysis, as shown in Fig. 5. Two layers of piezoelectric ceramics (type PZT-5A) with same thickness are deposited in the same direction of polarization while closely adhered to each intermediate electrode layer (i.e. cantilever substrate). The material of the intermediate electrode layer is brass. Wires were soldered upon the PZT surfaces for voltage output realization. The internal piezoelectric cantilever has a permanent magnet (A) (type N35), fixed to its free end while its root is fixed to Base 1. Meanwhile, Base 1 is fixed to the bottom plate of the device (i.e. Base 2), through which the entire energy converter receives excitations. The external piezoelectric cantilever has a permanent magnet (B) fixed to its free end while its root is fixed to Base 3, which is capable of moving horizontally along the length direction of the cantilever beams and Base 2 for adjustment of magnetic interval (*d*). The piezoelectric cantilever planes are parallel to Base 2 plane. Furthermore, in order to satisfy the assumption mentioned in Section II of not considering the magnets' gravity effect on the static deformation of the piezoelectric cantilever beams, the planes of the two cantilevers and Base 2 are deposited perpendicularly to the ground, while the exciter vibrates Base 2 along a direction parallel to the ground.

The schematic of the experimental test system is shown in Fig. 6, which is mainly composed of an arbitrary waveform generator (AWG), a power amplifier, an exciter, a DPEH, a laser doppler vibrometer (LDV), data acquisition system (DAQ), and a computer.[33, 38] In the experiment, a variety of realistic ambient noise recordings supplied by a professional sound effects library (*McKinney Sound*) were reproduced by the signal generator to imitate corresponding ambient conditions. Noise excitation signals acted on the energy converter through the power amplifier and the exciter, leading to vibrations of the piezoelectric cantilevers. Displacement and voltage output was respectively measured via LDV and DAQ then consequently transferred into a computer for analysis.

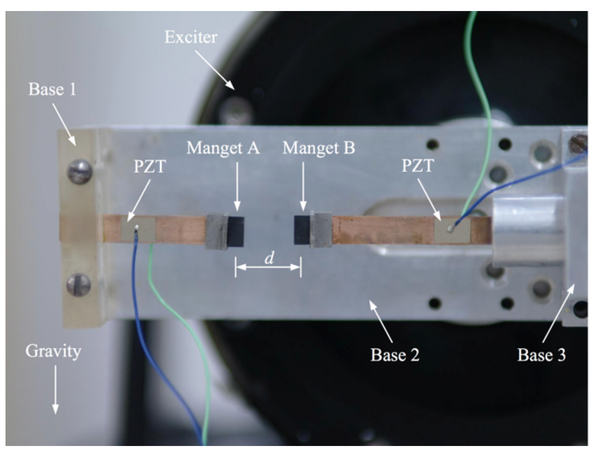

FIG. 5. Experimental setup.

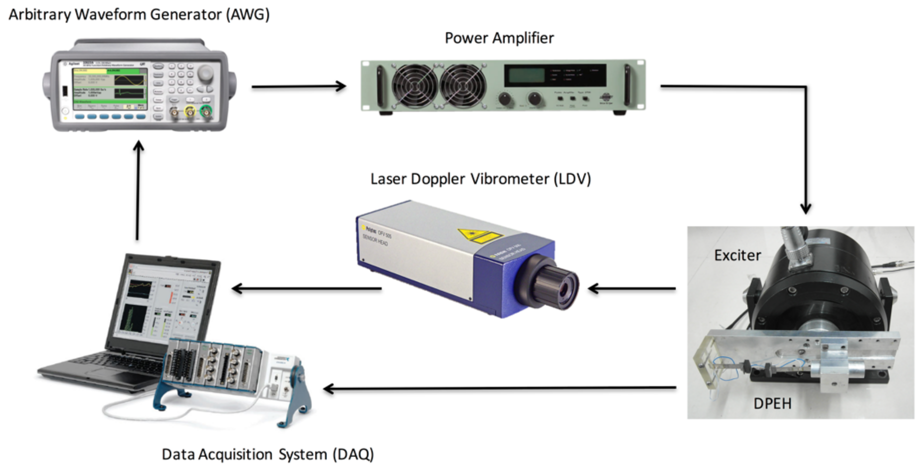

FIG. 6. Schematic of the experimental test system.

For ease of comparison, we categorized all types of ambient noises by the percentage of noise intensity variation, which is specifically represented in this paper by the percentage of sound pressure level variation of the realistic ambient noise recordings. Sound pressure level (SPL) is a logarithmic measure of the effective pressure of a sound relative to a reference value.[39, 40] It reflects the intensity of a sound because of the proportionality to frequency and amplitude. Given this, SPL variation is used hereafter as an indicator of the noise intensity variation in the following discussion. It should be noted that SPL variation is calculated in this paper using the maximum and the baseline value of SPL. A-weighting is adopted in this paper for the SPL measurement of the realistic ambient noise recordings. A-weighting is the most commonly used curve defined in the International standard IEC 61672:2003 and various national standards relating to the measurement of sound pressure level.[41, 42] In this paper, the calculation of A-weighting SPL is based on a calibrated 94dB pure tone with 1000 Hz.

According to Ref. 31-33 and Ref. 43, a set of fixed parameters including material properties (see Table 1) and geometries (see Table 2) were chosen for analysis. It should be noted that the length (l_e), width (w_e) and thickness (t_e) of the internal and external piezoelectric film are respectively the same. The rms output voltage of the two piezoelectric beams (V_{a_rms}, V_{b_rms}) is a suitable indicator of the power deliverable to the purely resistive load R.[12, 23] The rms output voltage of the entire system is followed by $V_{\text{rms}} = V_{a\_\text{rms}} + V_{b\_\text{rms}}$. The average electrical power produced by the piezoelectric oscillators is calculated by the formula $P_{\text{avg}} = {V_{\text{rms}}}^2/R$.[13, 21] We observed the variation of average electrical power (P_{avg}) with respect to the intensity variation of the vibration input, the interval of the two magnets (d), and the length of the external cantilever (l_b). Note that adjustment of l_b equals to adjustment of the external magnet's support state.[25] The less that l_b is, the closer the external magnet is to rigid-supported state. When $l_b = 0$, the entire system can be seen as rigid-supported. In contrast, the greater that l_b is, the closer the system is to elastic-supported state. The optimal values of model parameters of l_b and d are recommended by observing the energy harvesting performance under pink noise, whose noise intensity is determined by the maximum noise intensity of the assigned realistic noise. The reason why we select this method to estimate optimal parameters is that the energy harvesting convertors should be designed to make more use of high-intensity conditions in specific ambient areas. Other than considering this, the noise intensity baseline and noise intensity variation of specific ambient noises are assumed to be relatively constant toward given time.

Table 1. Material properties for DPEHS.

Parameter (Symbol)	Value
Elasticity modulus of cantilever substrate (E_a, E_b)	100 GPa
Elasticity modulus of piezoelectric ceramic (E_e)	66 GPa
Density of cantilever substrate (ρ_a, ρ_b)	$7165\ \mathrm{kg \cdot m^{-3}}$
Density of piezoelectric ceramic (ρ_e)	$7800\ \mathrm{kg \cdot m^{-3}}$
Density of permanent magnet (ρ_A, ρ_B)	$7500\ \mathrm{kg \cdot m^{-3}}$
Permeability of vacuum (μ_0)	$4\pi \times 10^{-7}\ \mathrm{N \cdot A^{-2}}$
Residual flux density (B_r)	1.25 T
Piezoelectric constant (d_{31})	$-190\ \mathrm{pC \cdot N^{-1}}$
Relative permittivity (ε_{31})	1500
Vacuum permittivity (ε_0)	$8.854\ \mathrm{pF \cdot m^{-1}}$

Table 2. Geometries for DPEHS.

Parameter (Symbol)	Value /mm
Length of internal cantilever substrate (l_a)	60
Length of piezoelectric film (l_e)	15
Thickness of permanent magnet (l_A, l_B)	5
Width of cantilever substrate (w_a, w_b)	10
Width of piezoelectric film (w_e)	8
Width of permanent magnet (w_A, w_B)	10
Thickness of cantilever substrate (t_a, t_b)	0.3
Thickness of piezoelectric film (t_e)	0.27
Height of permanent magnet (h_A, h_B)	8

According to the percentage of intensity variation, the realistic ambient noise recordings are categorized into three main groups: Significant-Variation Group, Medium-Variation Group and Constancy Group. To begin with, significant noise intensity variation can be normally caused by transportation such as cars, buses, motorcycles or trains when passing by certain spots. Thus, we analyzed using those type of noises and exhibit the performance under the most representative two noise recordings to summarize general regulations, as shown in Table 3. Corresponding SPL graphs of the realistic ambient noise recordings are attached for better comprehension. In each graph, there exists three SPL curves, respectively, drew upon calculations in time domain (blue), frequency domain (red) and using A-weighting method (green) [41, 42]. As has been mentioned above that A-weighting is the most commonly used curve for SPL measurement, hereafter we will be using A-weighting SPL values for analysis. One noise recording in Table 3 is from the town traffic at night and the other one is from the main road traffic. The common part of those two noises is that the background noises are faint enough to guarantee high intensity variation.

The output performance of DPEHS is illustrated by the phase diagram and the percentage of output power variation (ΔP_{avg}) compared to RPEHS.[25] For each specific case, the optimal values of model parameters of l_b and d are assigned according to the estimation method clarified above. As apparently shown in the phase diagrams of Table 3, biastable oscillation phenomenon would be more easily to occur in DPEHS during the significant intensity variation process, while RPEHS spent most of the time on weak oscillations in one well, which verified the superiority of dual-bistability with varying potential functions in transition probability enhance. On the other hand, when it comes to ΔP_{avg}, it has to be noticed in advance that since DPEHS has one more pair of piezoelectric patches than RPEHS, as a control, we launched another indicator of ΔP_{avg} between EPEHS and RPEHS, two of which have the same amount of piezoelectric films. Thanks to more frequent biastable oscillation phenomenon, both EPEHS and DPEHS are superior to RPEHS, which demonstrated that the EPEHS is more adaptive to realistic ambience with significant intensity variation than RPEHS, while DPEHS making the most of the dual piezoelectric cantilevers as electromechanical energy conversion to accomplish optimal energy harvesting. It should also be clarified that even though the intensity variation of two noise recordings are the same, the value of ΔP_{avg} might be different, since the intensity variation we discussed is the difference between the maximum and the baseline value of intensity, while nevertheless, all the other information carried by the noise, such as intensity varying performance, might be extremely different. Under such circumstance, no trend of the value of ΔP_{avg} could be certainly followed among different noise recordings. It would be only used as an indicator for superiority validation under exact same conditions.

Table 3. Output performance toward realistic ambience with significant intensity variation.

Input			Output			
Description	SPL Graph	Intensity Variation /%	RPEHS	DPEHS	ΔP_{avg} /%	
					EPEHS	DPEHS
Town Traffic at Night	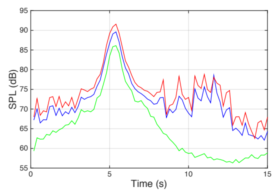	52.9	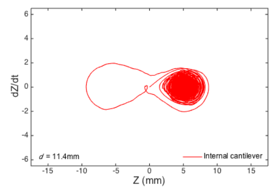	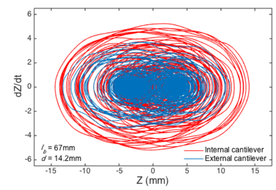	607.4	2044.0
Main Road Traffic	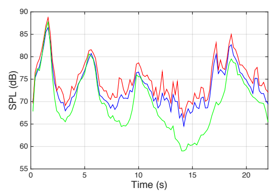	48.7	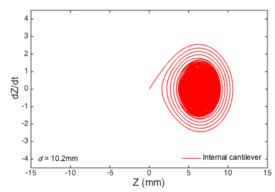	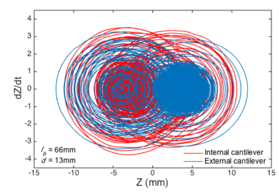	329.6	1574.4

Actually not all ambience has drastic intensity variation like the first group does. Most of the other realistic ambient noises belong to Medium-Variation Group. Those noises can be further classified according to locations including but not limited to: a) Interior of vehicles, such as cars or buses driving under variable road conditions; b) Busy outdoor public places, such as city streets or town squares with traffic and pedestrians around; c) Noisy indoor public places, such as departure/arrival halls in airports or shopping malls; d) Noisy areas near machines, such as baggage reclaims in airports or construction sites in streets. We analyzed using those type of noises and exhibit the performance under the most representative four noise recordings to summarize general regulations, as shown in Table 4. It can be realized that same as the first group, both EPEHS and DPEHS are superior to RPEHS, which could still not overcome the limit of single-well oscillations. Therefore, it is illustrated that EPEHS is more adaptive to realistic ambience with medium intensity variation than RPEHS, while DPEHS making the most of the dual piezoelectric cantilevers as electromechanical energy conversion to accomplish optimal energy harvesting.

Table 4. Output performance toward realistic ambience with medium intensity variation.

Input			Output			
Description	SPL Graph	Intensity Variation /%	RPEHS	DPEHS	ΔP_{avg} /%	
					EPEHS	DPEHS
Bus Interior, New York City	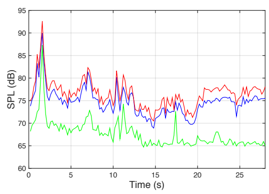	34.9	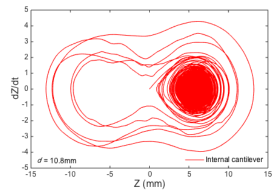	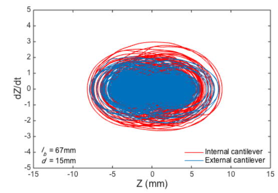	95.0	1463.2
Traffic and Pedestrians, New York City	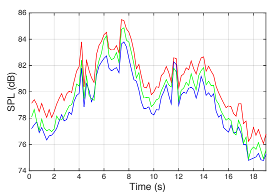	13.3	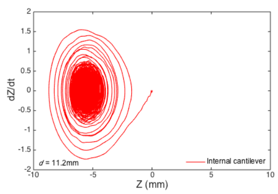	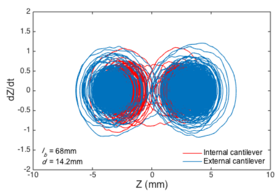	25.2	615.3
Arrivals Hall, Airport Heathrow	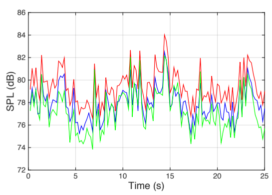	11.4	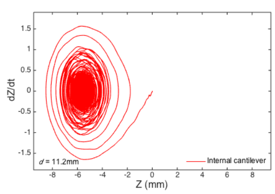	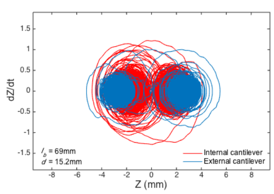	27.6	623.9
Baggage Reclaim, Airport La Rochelle	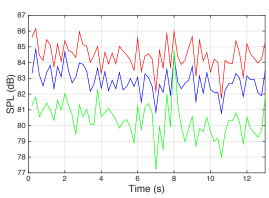	9.8	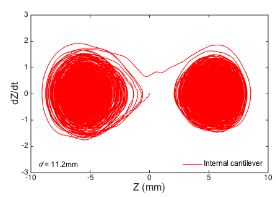	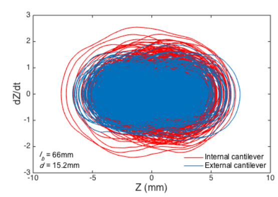	119.2	601.1

There are also a kind of ambient noises which are consist of relatively constant intensity components. Those noises are known caused by some major excitations with constant spectrum and intensity while in the meantime rarely being influenced by any other excitations. In terms of Constancy Group, we focus on areas like aircraft interior or plant ambience, which could also be simply acknowledged as background noise ambience. We analyzed using those type of noises and exhibit the performance under the most representative two noise recordings to summarize general regulations, as shown in Table 5. It should be noted that different from the situations of the other two groups discussed above, EPEHS received lower output power than RPEHS in this one for the latter managed to accomplish bistable oscillations. It is revealed from such phenomenon that EPEHS is less qualified in the realistic ambience with constant intensity than RPEHS. Fortunately, DPEHS is still superior to RPEHS due to the dual piezoelectric cantilevers of being efficiently utilized for electromechanical energy conversion so as to accomplish optimal energy harvesting.

Table 5. Output performance toward realistic ambience with constant intensity.

Input			Output			
Description	SPL Graph	Intensity Variation /%	RPEHS	DPEHS	ΔP_{avg} /%	
					EPEHS	DPEHS
Aircraft Boeing 737-800 Interior	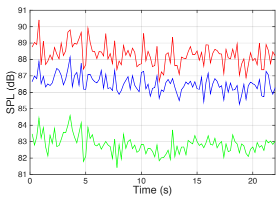	3.9	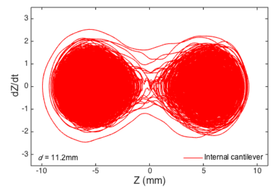	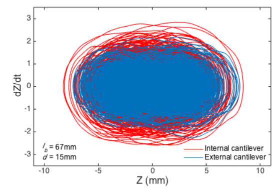	-35.2	160.5
Heavy Constant Industry Roar	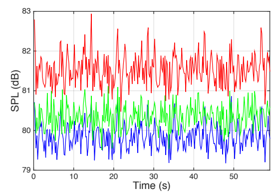	1.9	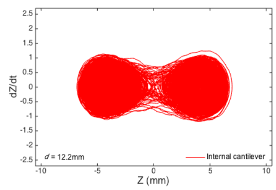	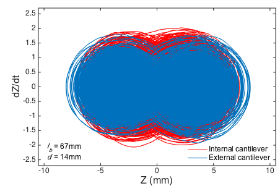	-22.2	274.8

4. Conclusion

Even though pink noises are known similar to realistic ambient noises, they could only be used for simulation on excitations that are assumed to own constant intensity. Nevertheless, realistic ambient noises normally come along with random spectrum and varying intensity in terms of different locations and time period. Unfortunately, the power performance of the conventional bistable magnetic repulsion harvesters would be significantly affected by the intensity of ambience. Considering this, a model of bistable DPEH is established in this paper to achieve optimal broadband energy harvesting toward varying-intensity realistic circumstance. Since it has already been proven in our previous work that EPEHS is adaptive to filtered Gaussian noises or pink noises with variable intensity, in this paper, we utilized a variety of realistic ambient conditions as excitations to obtain the energy harvesting performance of DPEHS for theoretical and applied study. It has been verified that EPEHS is more adaptive to realistic ambience with significant or medium intensity variation, while less qualified toward the realistic ambience with constant intensity than RPEHS. Fortunately, DPEHS are superior to RPEHS under all circumstance due to the dual piezoelectric cantilevers of being efficiently utilized for electromechanical energy conversion so as to accomplish optimal energy harvesting.

Acknowledgements

This work is supported by the National Natural Science Foundation of China (Grant No. 51275336) and the Tianjin Research Program of Application Foundation and Advanced Technology (Grant No.15JCZDJC32200). Y. Gao acknowledges support from the China Scholarship Council (File No. 201406250097). The realistic ambient noise recordings are supplied by *McKinney Sound* (http://www.freesfx.co.uk/users/mckinneysound).

References

[1] Friswell M I and Adhikari S 2010 Sensor shape design for piezoelectric cantilever beams to harvest vibration energy *J. Appl. Phys.* **108** 014901.

[2] Lefeuvre E, Badel A, Richard C, Petit L and Guyomar D 2006 A comparison between several vibration-powered generators for standalone systems *Sensors Actuators* A **126** 405-16.

[3] Harne R L and Wang K W 2013 A review of the recent research on vibration energy harvesting via bistable systems *Smart Mater. Struct.* **22** 023001.

[4] Tang L, Yang Y and Soh C K 2010 Toward broadband vibration-based energy harvesting *J. Intell. Mater. Syst. Struct.* **21** 1867-97.

[5] Zhu D, Tudor M J and Beeby S P 2009 Strategies for increasing the operating frequency range of vibration energy harvesters: a review *Meas. Sci. Technol.* **21** 022001.

[6] Ramlan R, Brennan M J, Mace B R and Kovacic I 2010 Potential benefits of a non-linear stiffness in an energy harvesting device *Nonlinear Dyn.* **59** 545-58.

[7] Mann B P and Sims N D 2009 Energy harvesting from the nonlinear oscillations of magnetic levitation *J. Sound Vib.* **319** 515-30.

[8] Sebald G, Kuwano H, Guyomar D and Ducharne B 2011 Experimental Duffing oscillator for broadband piezoelectric energy harvesting *Smart Mater. Struct.* **20** 102001.

[9] Erturk A, Hoffmann J and Inman D J 2009 A piezomagnetoelastic structure for broadband vibration energy harvesting *Appl. Phys. Lett.* **94** 254102.

[10] Zhao S and Erturk A 2013 On the stochastic excitation of monostable and bistable electroelastic power generators: relative advantages and tradeoffs in a physical system *Appl. Phys. Lett.* **102** 103902.

[11] Cottone F, Vocca H and Gammaitoni L 2009 Nonlinear energy harvesting *Phys. Rev. Lett.* **102** 080601.

[12] Ferrari M, Ferrari V, Guizzetti M, Andò B, Baglio S and Trigona C 2010 Improved energy harvesting from wideband vibrations by nonlinear piezoelectric converters *Sensors and Actuators A: Physical* **162** 425-31.

[13] Stanton S C, McGehee C C and Mann B P 2010 Nonlinear dynamics for broadband energy harvesting: Investigation of a bistable piezoelectric inertial generator *Physica D: Nonlinear Phenomena* **239** 640-53.

[14] Mann B P and Owens B A 2010 Investigations of a nonlinear energy harvester with a bistable potential well *J. Sound Vib.* **329** 1215-26.

[15] Cottone F, Gammaitoni L, Vocca H, Ferrari M and Ferrari V 2012 Piezoelectric buckled beams for random vibration energy harvesting *Smart Mater. Struct.* **21** 035021.

[16] Liu W Q, Badel A, Formosa F, Wu Y P and Agbossou A 2013 Novel piezoelectric bistable oscillator architecture for wideband vibration energy harvesting *Smart Mater. Struct.* **22** 035013.

[17] Leadenham S and Erturk A 2015 Nonlinear M-shaped broadband piezoelectric energy harvester for very low base accelerations: primary and secondary resonances *Smart Mater. Struct.* **24** 055021.

[18] Arrieta A F, Hagedorn P, Erturk A and Inman D J 2010 A piezoelectric bistable plate for nonlinear broadband energy harvesting *Appl. Phys. Lett.* **97** 104102.

[19] Gammaitoni L, Neri I and Vocca H 2009 Nonlinear oscillators for vibration energy harvesting *Appl. Phys. Lett.* **94** 164102.

[20] Erturk A and Inman D J 2011 Broadband piezoelectric power generation on high-energy orbits of the bistable Duffing oscillator with electromechanical coupling *J. Sound Vib.* **330** 2339-53.

[21] Vocca H, Neri I, Travasso F and Gammaitoni L 2012 Kinetic energy harvesting with bistable oscillators *Appl. Energy* **97** 771-76.

[22] Daqaq M, Masana R, Erturk A and Quinn D 2014 On the role of nonlinearities in vibration energy harvesting: a critical review and discussion *ASME Applied Mechanics Reviews* **66** 040801.

[23] Ferrari M, Baù M, Guizzetti M and Ferrari V 2011 A single-magnet nonlinear piezoelectric converter for enhanced energy harvesting from random vibrations *Sensors and Actuators* A **172** 287-92.

[24] Gao Y J, Leng Y G, Fan S B and Lai Z H 2014 Studies on vibration response and energy harvesting of elastic-supported bistable piezoelectric cantilever beams *Acta Phys. Sin.* **63** 090501.

[25] Leng Y G, Gao Y J, Tan D, Fan S B and Lai Z H 2015 An elastic-support model for enhanced bistable piezoelectric energy harvesting from random vibrations *J. Appl. Phys.* **117** 064901.

[26] Bak P, Tang C and Wiesenfeld K 1987 Self-organized criticality: An explanation of the 1/f noise *Phys. Rev. Lett.* **59** 381-84.

[27] Hooge F N 1994 1/f noise sources *IEEE T. Electron Dev.* **41** 1926-35.

[28] Halley J M and Kunin W E 1999 Extinction risk and the 1/f family of noise models *Theor. Popul. Biol.* **56** 215-

30.

[29] Gao Y J, Leng Y G, Fan S B and Lai Z H 2014 Performance of bistable piezoelectric cantilever vibration energy harvesters with an elastic support external magnet. *Smart Mater. Struct.* **23** 095003.

[30] Priya S and Inman D J Eds 2009 *Energy harvesting technologies* (New York: Springer) **21**.

[31] DuToit N E and Wardle B L 2005 Design considerations for MEMS-scale piezoelectric mechanical vibration energy harvesters *Integr. Ferroelectr.* **71** 121-60.

[32] Ali S F, Adhikari S, Friswell M I and Narayanan S 2011 The analysis of piezomagnetoelastic energy harvesters under broadband random excitations *J. Appl. Phys.* **109** 074904.

[33] DuToit N E and Wardle B L 2007 Experimental verification of models for microfabricated piezoelectric vibration energy harvesters *AIAA Journal* **45** 1126-37.

[34] Leng Y G, Leng Y S and Wang T Y 2006 Numerical analysis and engineering application of large parameter stochastic resonance *J. Sound Vib.* **292** 788-801.

[35] Leng Y G, Wang T Y, Guo Y, Xu Y G and Fan S B 2007 Engineering signal processing based on bistable stochastic resonance *Mechanical Systems and Signal Processing* **21** 138-50.

[36] Leng Y G 2011 Mechanism of high frequency resonance of parameter-adjusted bistable system *Acta Phys. Sin.* **60** 020503

[37] Villani D D 1998 An analytic solution for the force between two magnetic dipoles *Magnetic and electrical Separation* **9** 39-52.

[38] Stanton S C, Erturk A, Mann B P and Inman D J 2010 Nonlinear piezoelectricity in electroelastic energy harvesters: modeling and experimental identification *J. Appl. Phys.* **108** 074903.

[39] Beranek L L 1993 *Acoustics* (New York: Acoustical Society of America).

[40] Raichel D R 2006 *The Science and Applications of Acoustics* (New York: Springer Science & Business Media).

[41] Smith M T Ed 2001 *Audio Engineer's Reference Book, 2nd Edition* (Focal Press).

[42] Moore B C J 2003 *An Introduction to the Psychology of Hearing, 5th Edition* (Academic Press).

[43] Roundy S, Wright P K and Rabaey J 2003 A study of low level vibrations as a power source for wireless sensor nodes *Comput. Commun.* **26** 1131-44.